Inspection of Ground Embedded Runway Lights through Monoscopic Camera via Mobile Robotics

Anders Christoffersen
agch20@student.aau.dk

Kasper Jensen
kjense16@student.aau.dk

Bjarne Johannsen
bjohan20@student.aau.dk

Frederik Larsen
flarse17@student.aau.dk

Jan Przybyszewski
jprzyb20@student.aau.dk

Rares Ungureanu
rungur17@student.aau.dk

***Abstract*—The aim of this paper was to investigate the potential of an automated solution for inspection of ground-embedded runway-lights, with no humans-in-the-loop. A prototype differential-drive mobile robot featuring two monoscopic cameras, communicating with a database of positions from ground-embedded runway-lights was built and tested on an airport. Tests indicated promising results for further research and expansion of the current robotic-platform-solution as a functional and viable solution for automatic inspection of runway-lights. Accuracy test requirements demanded a maximum distance error of 15 meters with a maximum angular error of 2.9°. Results showed the robot was able to maneuver around a predefined path with a mean heading angular error of 1.6 °. Runway light-detection test of a set of 58 runway-lights concluded on a 6 meter accuracy, with a maximum angular error of 1.7°. Both of these results within the required specifications. The significance of these results demonstrate the viability of this paper's robotic system in runway light-detection within minimum specification, as well as usage of the detection methods to determine which lights need human intervention for replacement or maintenance.**

I. Introduction

Thousands of planes land every day in airports around the world [1]. In order to navigate the runways, indicator lights for landing zones and taxi routes are necessary. Failure in lighting can result in catastrophic failure in plane navigation. Runway light inspection is therefore necessary and required by regulation, with this procedure currently being done manually in airports around the world. Manual inspection of runway lights is done by driving to all light locations and verifying colour, intensity, functionality, and visibility [2]. Issues of this method are the monotonous nature of the task, leading to possible human errors, along with the associated dangers of unnecessary travel on the runways of an active airport. Automated inspection of airport runways currently only pertains to pavement crack detection and detection of debris on the runway [3]. This work was unable to find a fully automated solution of both the inspection robot without humans-in-loop or any literature on automated runway light detection. This paper therefore presents a novel full stack solution for inspection of airport runway lights via two monoscopic cameras mounted on the front and rear of a prototype Autonomous Mobile Robot platform (AMR). The focus of this paper will be an autonomous platform for the detection and database association of ground embedded circular lights, with a diameter of 30 cm, placed on the taxiway and runway of Aarhus Airport. The location of these lights will be associated to the position of an existing database, with the intent of affirming whether the light is visible at the location and afterwards calculating a confidence score. Summarized in section II is the overall system architecture along with the specifications and theories of the subsystem components. Section III presents the test descriptions along with results of the tested parts of the implementation. The paper is concluded in section IV.

II. Methods and Materials

A. System Architecture

The system architecture of the autonomous runway inspection robot has been designed for reliability, modularity, and performance. The robot platform is equipped with an inertial measurement unit with a magnetometer (IMU). Individual wheel speeds are determined by reading out an encoder on each wheel. High precision Global Navigation Satellite System (GNSS) is used in conjunction with real time kinematics as a position sensor. Lights are detected by both frontal and rear cameras in order to inspect both sides in a single pass and reduce the inspection time. The camera images are processed, the center of the light hypotheses are extracted and the relative position to the camera frame is estimated. The hypotheses are then associated to the known database and the light status is updated.

The chosen computing system consists of a high performance embedded application computer and a low power autonomous control unit. The application control unit is dedicated to vision-based perception and all relevant application processes. The autonomous control unit runs all other software packages that keep the robot functional even without the application control unit. All processing units communicate via Ethernet. The designed software system runs on the ROS Noetic framework. NTP is used to synchronize the clocks of all processing units the local network. The autonomous control unit also runs the low level controllers and low level state machine of the robot platform. The state estimation predicts an accurate high frequency pose for the trajectory controller and the light association. In order to follow the global path, the trajectory control and motor control work together and control the motors. Furthermore, a state machine controls the current

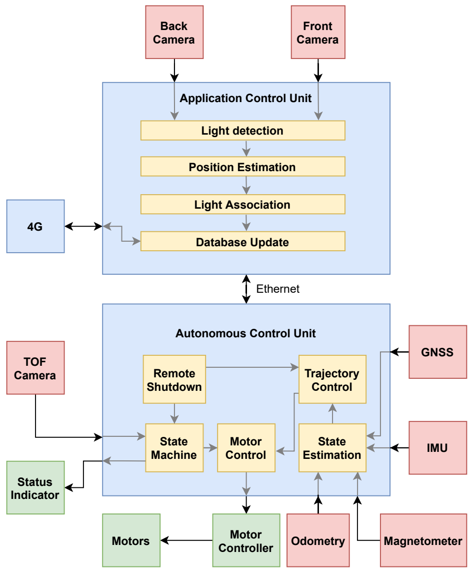

Fig. 1. Overview of the autonomous system architecture.

state of the robot and is able to disengage the motors in case of an unexpected obstacle detected by the front time-of-flight camera, which is monitoring the area in front of the robot. In case of an emergency the remote shutdown can generate an safe trajectory to leave the runway as fast as possible and come to a safe stop. The different states are visualized by the autonomous system status indicators.

B. Hardware Specification

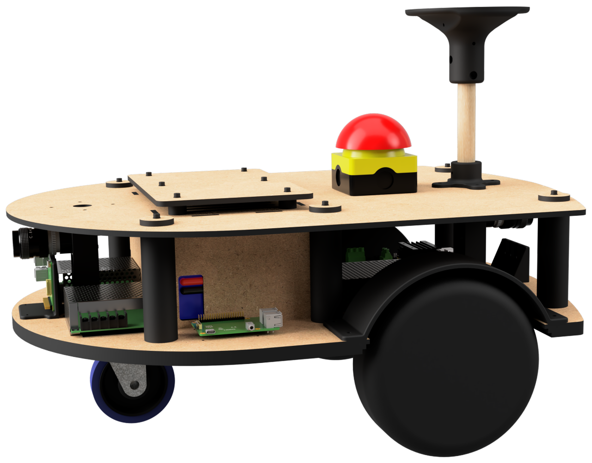

Fig. 2. Render of finished AMR with most significant components

As seen in Fig. 2, the robot is designed as a prototype differential drive AMR platform. The AMR features an high power motor controller for two 600W wheel hub motors, and a selection of embedded computing hardware acting as a distributed system by using ROS (Robot Operating System) as a middleware. An Nvidia Jetson Nano representing the application control unit is able to process images from both a front and rear a camera at 20 Hz and therefore operating at the full frame rate of the cameras with a given shutter time of 50ms for the best possible raw image at night. Due to the known geometric relationships and the runway, which is assumed to be a plane, a mono camera pipeline is used. In order to be able to inspect both sides of the runway lighting in a single run, one camera each at the front and rear is used. Due to the width of the runway, approximately 60 meters, the widest available lens of 6mm is used. Camera models are UI-3070CPC-HQ Rev.2 and UI3140CPC-HQ Rev.2 from IDS. By taking the given measures into account, the minimal depth and angular resolution can be derived. Resulting in a maximum depth error of 15m and angular error requirement of 2.9°. For trajectory planning and state estimation, a Raspberry Pi 4 has been utilized as the autonomous control unit. An additional Raspberry Pi 4 is placed with a 3D time-of-flight sensor in the front end of the robot with embedded point cloud processing, acting as a safety precaution for the robot and surroundings. Figure 2 shows the proposed differential drive robot with integrated cameras and GNSS.

The IMU and GNSS devices experienced system-breaking electrical noise disruptions when the motor controllers were engaged in closed loop control mode. MK II presents design changes to counter those issues. Full change log is to be found in the edited worksheets.

C. Light detection

The process of detecting lights on the runway is split into two main steps:

- Position estimation: Images are taken from the camera and processed, contours of the lights are found and their centers are transformed via a homography matrix to relative meters in the robot's GNSS perspective, along with an uncertainty ellipsoid. Due to the positioning of the lights on the runway and their distance relative to one another (150 cm between lights situated on the same row, 3000 cm between rows of lights), this operation will be considered accurate if the estimation of the X coordinate has an error lower than 75 cm and the estimation of the Y coordinate has an error lower than 1500 cm.
- Database matching: The relative coordinates are converted to latitude and longitude coordinates by using the position given by the robot's GNSS, the estimated coordinates and uncertainty ellipsoid are used to match the light to it's correspondent in the local database.

The front and rear camera follow the same exact computer vision pipeline, ran in parallel on the robot's onboard computer.

1) Position estimation: After acquisition, the camera image is undistorted using a transformation matrix and distance coefficients obtained in a prior checkerboard camera calibration. Since the light inspection operation is performed at night when there is a low level of ambient light, lights can be distinguished from other elements in a grey-scale image due to their high pixel intensity. However, other lights than those on the runway can be present in an image, such as those from the airport buildings surrounding the runways. These lights appear mainly around and above the horizon line, while the lights of interest appear below the horizon as they are embedded in the ground. Additionally, lights on the runway appear increasingly close to each other and eventually have their contours merge, as they are farther away from the camera and closer to the vanishing point. To solve both issues, the image is cropped to a set height that allows for distinction between separate light contours and eliminates irrelevant lights, as seen in Fig. 3.

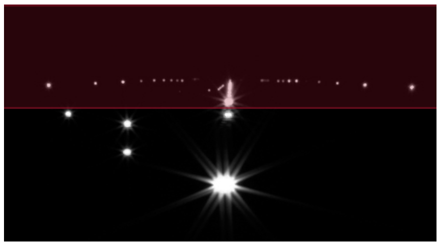

Fig. 3. Grey-scale image of lights on the runway, with the red area representing the part of the image that is undesirable and discarded in the crop.

An intensity threshold is applied to the cropped image to remove any potential noise and reduce the image to black and white pixels only. This image binarization reduces the problem to finding the contours of the lights, in order to further calculate the coordinates of its center pixel. For this task, two of the most popular contour tracing and pixel clustering algorithms were tested for performance: the Suzuki contour tracing algorithm [4] and the DBSCAN clustering algorithm [5]. The Suzuki algorithm was chosen for this project's implementation as it outperformed the latter by 13.3ms in runtime while still detection all lights correctly. The pixel coordinates of the contour's center are transformed into relative meter camera coordinate frame with the use of a homography transformation. The homography transformation matrix was determined in a prior calibration of the computer vision setup by capturing an image of a rectangle of known real world dimensions and mapping it's corners to the corresponding pixel coordinates in the image, Fig. 4. With 4 pairs of pixel-meters vertices, the 3x3 matrix is found by a process of Gaussian elimination.

Because this solution cannot directly obtain the perfect absolute position of a light in a non deterministic system such as a mobile robot, the algorithm also estimates the uncertainty by transforming the known uncertainty in image coordinates to the real world. This will result in an uncertainty ellipsoid which is used to associate light correctly. The homography transformation matrix is multiplied with the center pixel of the light's contours and it's uncertainty pixels as follows:

$$x_{ground} = \mathbf{H} \cdot x_{image} \tag{1}$$

where x_{ground} and x_{image} are vertices in the ground and image plane respectively, and $\mathbf{H}$ is the homography transformation matrix. The light's relative meters position from the robot and uncertainty ellipsoid are then passed on to the next stage of light detection.

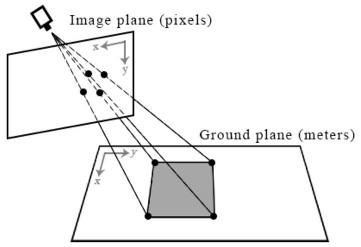

Fig. 4. A rectangle on the ground plane with it's corners being mapped to pixels onto the image plane. This is a homography transformation of the corners from the ground plane to the image plane.

2) Database association: After successful detection and transformation of the light's relative meters position into a globally fixed coordinate frame, it is necessary to associate it with the database. Figure 5 visualizes this process.

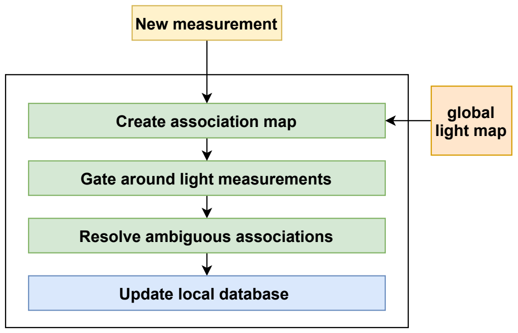

Fig. 5. Flow diagram of the database association.

When new measurements arrive, an association map is created with the globally known lights. Based on the positional inaccuracy of the robot and the uncertainty of the light detection, an elliptical gating area is formed as shown in figure 6. Ambiguous associations are resolved by computing the association cost using the Mahalanobis distance and a nearest neighbour search. Due to the calculated statics of the light at the end it is possible to use this technique as long as the majority of associations are correct.

After the correct association to the known map, the local database is updated with detected and expected detections.

D. Path Planning and Control

The kinematic model employed is the differential drive model. The model consists of 2 drive wheels, which are sharing a common axis. Each wheel can be independently driven in both directions. With such a kinematic model robot can turn by varying the difference in velocities of the two wheels, as well as obtain a straight line trajectory, by setting equal velocities to both wheels.

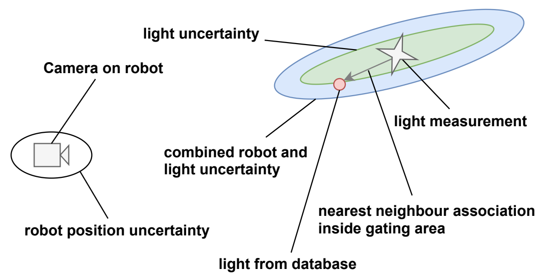
light uncertainty
Camera on robot
light measurement
combined robot and light uncertainty
robot position uncertainty
nearest neighbour association inside gating area
light from database
Fig. 6. Visualisation of the gating area and association relative to the camera.

The controller node controlling the robot's wheels receives a standard ROS command velocity message, which consists of 3 linear and 3 angular velocity values $v_x, v_y, v_z, \omega_x, \omega_y, \omega_z$. The values are using the robot's local coordinate frame. After receiving velocities from the message, the node proceeds to compute demanded angular velocity of the wheels. Given the robot's velocity v_{rob} in the x_{rob} direction, the angular velocity ω_{rob} around the z axis, the robot tire radius r and the robot wheel track $2R$, the equations used to obtain angular velocity for each wheel (ω_l, ω_r) are presented below:

$$v_{wheel} = \omega_{rob} \cdot R \tag{2}$$
$$\omega_l = \frac{(v_{rob} - \frac{v_{wheel}}{2})}{r}$$
$$\omega_r = \frac{(v_{rob} + \frac{v_{wheel}}{2})}{r}$$

Computed values are then transmitted to the motor controller, which uses a PID control algorithm for each motor to obtain demanded velocities.
Path following node is based on a tracker and a planner. Given a path of points in the map coordinate frame, the planner feeds goal points to the tracker. When the robot obtains a current goal point, the tracker switches the goal point to the next point on the path. The tracker makes use of the pure pursuit controller proposed by RC Coulter [6]. This control strategy is chosen based on several simulations with different paths. The candidate controller taken into account is also the LQR optimal control algorithm. After careful consideration, it is assumed that in most cases the inspection paths are constructed from straight lines. Simulation results for both controllers prove, that on such routes pure pursuit is the superior strategy obtaining mean tracking error lower by 0.2 meters and 2 times shorter computation time than it's counterpart. Pure pursuit is a geometry-based path tracking algorithm which computes the angular velocity value, to move the robot towards a point on the demanded path. The distance between the point and the robot is described by a tuning parameter - lookahead distance. The robot position in the map frame needed for computations is obtained from the localization node. The algorithm steps can be described as follows:

- Determine robot's position.
- Find the target point on the path, using the lookahead distance.
- Transform the target point to the robot's coordinate frame.
- Compute the curvature connecting robot's position and the target point.
- Calculate angular velocity.

In the proposed system a constant linear velocity is used. After the angular velocity value is computed by the tracker program, a Twist message is created and published to a topic subscribed by the controller node.

E. State Estimation

State estimation is an essential part of any mobile robotic application as it enables the robust operation of other system components, such as the trajectory control and runway light association. Several sensors are fused to estimate the pose and velocity of the ground robot. 7 shows the proposed architecture. With an output of the final pose in a locally consistent fixed frame, called map. To take advantage of redundancy in state estimation, the contribution of each sensor input to the overall estimated state has to be quantified in function of the sensor's accuracy and previous state knowledge. The Extended Kalman Filter (EKF) is the state-of-the-art estimator for fast, mildly non-linear systems. For systems with white zero-mean additive Gaussian noise corrupting the sensors and the process model, it is a good approximation of the optimal solution.

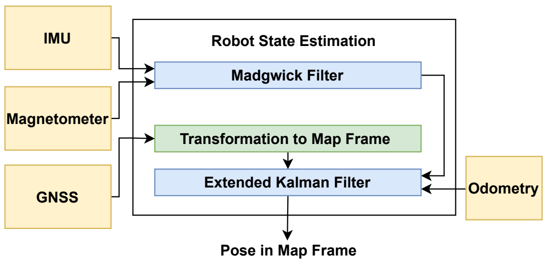

Fig. 7. Overview of the state estimation.

Madgwick's algorithm is applicable to inertial measurement units (IMU) consisting of gyroscopes and accelerometers sensor arrays that also include magnetometers. It shows a 36% lower orientation standard deviation error then Kalman-based approaches. [7] The algorithm uses a quaternion representation, This representation is numerically more efficient and required by the ROS common messages. Allowing accelerometer and magnetometer data to be used in an analytically derived and optimised gradient descent algorithm to calculate the direction of the gyroscope measurement error as a quaternion derivative. The orientation is calculated by two main processes. In the first step gyroscope measurements are processed with a correction algorithm, which

depends on the parameter ζ. To minimize the error caused by the bias and the drift, they are used to calculate the orientation with the quaternion propagation starting from the orientation estimated at the previous step. Afterwards the accelerometer and magnetometer measurements are fused with a tuning parameter β by the gradient descent algorithm, which defined in [8]. The output of the gradient descent algorithm is then used to correct the orientation estimated by considering only gyroscope measurements. In order to have reliable input for the Extended Kalman Filter the standard deviation of the fused 9-dof output is determined and set accordingly in the covariance matrices.

The process model for the extended kalman filter used is driven by the accelerometer as proposed in [9]. The robot base frame is chosen to carry the IMU which is placed in the center of rotation which is represented by the middle point between both powered wheels. A constant velocity model is used with the accelerometer as an input to the system. Due to the application constraints of a mobile robot on an airport runway, it is known that the vehicle will remain flat on the ground and not be significantly tilted. This assumption simplifies the state to a 2D state with only 6 elements. The state vector is defined as:

$$\begin{aligned} x &= [p^T, \theta, v^T, r]^T \qquad (3) \\ p &= [x, y]^T \\ v &= [v_x, v_y]^T \end{aligned}$$

p and θ are the position and heading of the mobile robot platform represented in the map frame. v and r are the linear and angular velocities of the robot represented in it's the base frame. The process model is defined as:

$$\begin{aligned} \dot{p} &= R(\theta)^T v \qquad (4) \\ \dot{\theta} &= r \\ \dot{v} &= a + [v_y r - v_x r]^T + n_v \\ \dot{r} &= n_r \end{aligned}$$

a is the measured acceleration, $R(\theta)$ the rotation matrix between the robot base frame and the fixed map frame. n_r and n_v represent white noise. The robot platform is equipped with multiple sensors which can be reduced to the quantities being measured: position z_p, heading z_θ, velocity z_v, and yaw rate z_r. For example the GNSS can be seen as an absolute position sensor. This holds only if it can be assumed that the noises of the decomposed measurements are uncorrelated. The measurements are defined as:

$$\begin{aligned} z_p &= h_p(x) = p + R(\theta)^T p_s + n_{z_p} \qquad (5) \\ z_\theta &= h_\theta(x) = \theta + \theta_s + n_{z\theta} \\ z_v &= h_v(x) = R(\theta_s)(v + [-r p_{s,y}, r p_{s,x}]^T) + n_{z_v} \\ z_r &= h_r(x) = r + n_{z_r} \end{aligned}$$

where $h(x)$ are the different measurement models and p_s the position of the sensor in base frame of the robot. θ_s is the sensor heading in base frame. Gaussian noises that introduce uncertainty in the sensor measurements are defined by n.

F. Database Communication

The AMR and local information about the runway relies on a database of points of interest maintained apart from the robot. While the database and access are application specific, it is expected that many airports to use a similar method of cataloging their lights to ensure appropriate inspections in accordance with runway maintenance guidelines. A copy of the database is downloaded to the robot from the origin source, and updated on the local version until the robot has completed a full inspection. The database information is downloaded over a wireless 4G cellular network to provide higher flexibility; this same connection is also used for GNSS correction data. Certain critical information is necessary, and made available to the other software on the robot. This includes the ID number of each light, model number, the WGS (World Geodesic System) coordinates of the light, and two extra fields added to the list by our method to provide an expected number of detections, and another to increment each time a valid detection is made. After the inspection is complete the number of times a light is seen is compared to the expected time to create a confidence score C with

$$C = \frac{T_{Seen}}{T_{Expected}}, \qquad V_{update} = \begin{cases} 0 & C < C_{Threshold} \\ 1 & C \geq C_{Threshold} \end{cases}$$

This confidence score is then compared to a set threshold for identification, if the light has been seen enough times that it can be reasonably verified to be in functioning condition, the status in the local database is updated. After each light's score has been checked against this threshold, the lights that can be ascertained to be functioning are sent back to the master database with an update code and status matching that which would indicate the appropriate time and manner of inspection. By using this technique small measurement errors can be compensated and and ambiguities compensated as long as the majority is correct and the threshold value adjusted accordingly. Therefore creating a robust and completely autonomous inspection system without any human operator.

III. Results

The proposed autonomous mobile robotic platform has been validated from subsystem to system level. Furthermore extensive tests on an actual airport have been conducted. The robot platform showed to be mechanically very stable with vibration introduced angular velocities of mostly below 0.05rad/s compared to more simple differential drive platforms with a critical x and y angular velocity of 5rad/s. There the proposed platform is capable of capturing long exposed images while driving in the night.

A. State Estimation

The following figure 8 shows the GNSS Measurements (blue) and estimated states in between (green) as well as the planned path (yellow). It can be seen that the full state estimation by using the Madgwick orientation estimation together with the EKF to estimate the corrected pose is able provide a low error base line for the pure pursuit controller to accurately follow the planned path. It shows an angular heading error of 1.5°. This test was conducted on the actual airport runway including all local conditions.

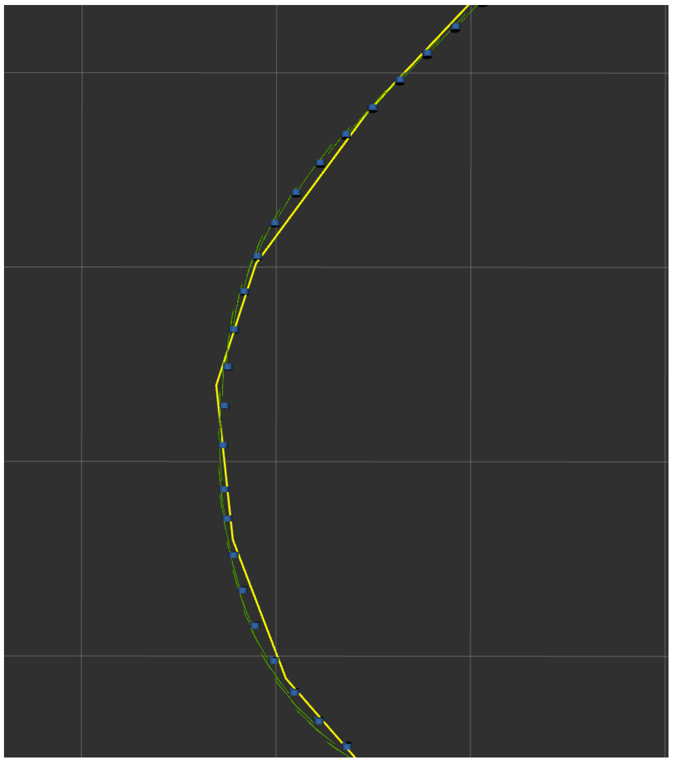

Fig. 8. Estimated Pose green arrow, RTK Updated blue cylinder and planned trajectory yellow in the most difficult corner on the airport.

B. *Runway Light Inspection*

Figure 9 shows the absolute light detection error as a function of the distance to the light. The validation of the light detection was performed by comparing the values estimated by the perception pipeline with known ground-truth values and calculating the error between them. It can be seen that the error stays way below the requirement of 15m while maintaining an angular error of 1.7°. Therefore resulting in a system error lower than all initial requirements to accurately associate the lights correctly.

IV. Conclusion

This presented paper presents a novel approach to autonomous runway light inspection. Obtained results show that modern mobile robots are capable of being employed in high-profile tasks. The proposed robotic platform can solve problems related to manual inspection done by human operators, increasing safety and repeat-ability. The described perception algorithms together with implemented localization and navigation stack proved to obtain sufficient light association accuracy. The robotic platform is flexible and can be used in different conditions.

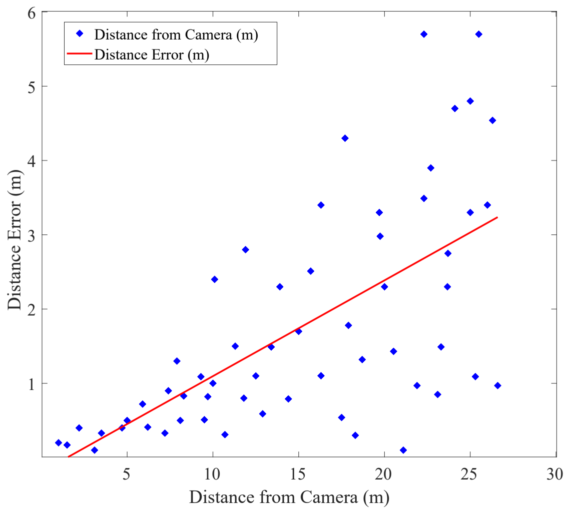

Fig. 9. Overview of the autonomous system's architecture.

Further research can be conducted, based on this work and the runway crack detection presented in [3], to develop a complete airport infrastructure inspection platform, which fully automates all inspections.

Acknowledgment

This work was partly supported by iLocator, Aarhus Airport, and Leica Geosystems.

References

[1] Federal Aviation Administration, "Air Traffic By Numbers," Air Traffic, 21-Sep-2020. [Online]. Available: https://www.faa.gov/air_traffic/by_the_numbers. [Accessed: 03-Dec-2020].

[2] L. Dragonas, "Inspection of Aerodrome Lighting," Federal Aviation Administration, Aerodrome Lighting Inspection of Aerodrome Lighting , 2012. [Online]. Available: https://www.icao.int/NACC/Documents/Meetings/2012/ICAOFAAAGACertification2012/ICAOFAACertification09.pdf. [Accessed: 08-Dec-2020].

[3] Z. Gui and H. Li, "Automated Defect Detection and Visualization for the Robotic Airport Runway Inspection," IEEE Access, vol. 8, pp. 76100–76107, Apr. 2020.

[4] S. Suzuki and K. Abe, "Topological structural analysis of digitized binary images by border following," Computer Vision, Graphics, and Image Processing, vol. 30, no. 1, pp. 32–46, 1985.

[5] Zheng Hua, Wang Zhenxing, Zhang Liancheng and Wang Qian, "Clustering algorithm based on characteristics of density distribution," 2010 2nd International Conference on Advanced Computer Control, Shenyang, 2010, pp. 431-435, doi: 10.1109/ICACC.2010.5486640.

[6] R. Craig Coulter, The Robotics Institute, Carnegie Mellon University, Pittsburgh, PA, tech., 1990.

[7] S. A. Ludwig and K. D. Burnham, "Comparison of Euler Estimate using Extended Kalman Filter, Madgwick and Mahony on Quadcopter Flight Data," 2018 International Conference on Unmanned Aircraft Systems (ICUAS), Dallas, TX, 2018, pp. 1236-1241, doi: 10.1109/ICUAS.2018.8453465.

[8] S. O. H. Madgwick, A. J. L. Harrison, and R. Vaidyanathan, "IEEE International Conference on Rehabilitation Robotics (ICORR) ," in Estimation of IMU and MARG orientation using a gradient descent algorithm.

[9] S. Lynen, M. W. Achtelik, S. Weiss, M. Chli and R. Siegwart, "A robust and modular multi-sensor fusion approach applied to MAV navigation," 2013 IEEE/RSJ International Conference on Intelligent Robots and Systems, Tokyo, 2013, pp. 3923-3929, doi: 10.1109/IROS.2013.6696917.